THE JOURNAL OF PHYSICAL CHEMISTRY Letters

pubs.acs.org/JPCL Letter

Near-Edge Ligand Stripping and Robust Radiative Exciton Recombination in CdSe/CdS Core/Crown Nanoplatelets

Jari Leemans, Shalini Singh, Chen Li, Stephanie Ten Brinck, Sara Bals, Ivan Infante, Iwan Moreels, and Zeger Hens*

Cite This: J. Phys. Chem. Lett. 2020, 11, 3339−3344 Read Online

ACCESS | Metrics & More | Article Recommendations | Supporting Information

ABSTRACT: We address the relation between surface chemistry and optoelectronic properties in semiconductor nanocrystals using core/crown CdSe/CdS nanoplatelets passivated by cadmium oleate ($Cd(Ol)_2$) as model systems. We show that addition of butylamine to a nanoplatelet (NPL) dispersion maximally displaces ~40% of the original $Cd(Ol)_2$ capping. On the basis of density functional theory simulations, we argue that this behavior reflects the preferential displacement of $Cd(Ol)_2$ from (near)-edge surface sites. Opposite from CdSe core NPLs, core/crown NPL dispersions can retain 45% of their initial photoluminescence efficiency after ligand displacement, while radiative exciton recombination keeps dominating the luminescent decay. Using electron microscopy observations, we assign this robust photoluminescence to NPLs with a complete CdS crown, which prevents charge carrier trapping in the near-edge surface sites created by ligand displacement. We conclude that Z-type ligands such as cadmium carboxylates can provide full electronic passivation of (100) facets yet are prone to displacement from (near)-edge surface sites.

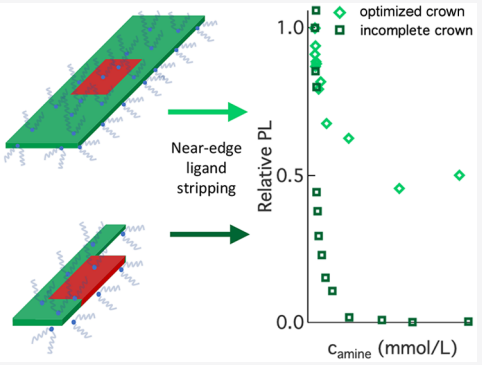

Colloidal semiconductor nanocrystals (NCs) make up a new class of optoelectronic materials that offer a combination of size-tunable optical properties and a suitability for solution-based processing.[1,2] Emerging applications in lighting and display rely on NCs for light emission, making the stability and efficiency of the NC photoluminescence a central research topic.[3] From this perspective, the large fraction of surface atoms in NCs is a drawback.[4,5] Undercoordinated surface atoms can have dangling bonds that lead to localized electronic states within the band gap, thereby providing efficient pathways for nonradiative recombination of electron−hole pairs. The formation of such trap states can be avoided by the passivation of undercoordinated surface atoms, either by the epitaxial overgrowth of an original core NC with a wide band gap semiconductor shell[6−9] or by the chemisorption of molecular ligands.[10−14] The latter point was recently confirmed in the case of CdSe NCs by theoretical studies of realistic model systems.[15,16] In particular, it was found that the desorption of Cd salts as Z-type ligands from the CdSe surface can leave behind dicoordinated surface Se atoms, which induce a localized, midgap state. The recent confirmation that saturating the NC surface with Z-type ligands can effectively lead to near unity photoluminescence quantum yields (PLQY) further highlights the underlying relation between the surface termination and the photoluminescence efficiency of NCs.[11,17]

Colloidal nanoplatelets (NPLs) make up a unique class of NCs. In the case of cadmium chalcogenides, NPLs with the zinc blende structure can be obtained as atomically flat, two-dimensional NCs featuring a singe, atomically precise layer thickness across the entire ensemble.[18−24] Because the NPL thickness determines the exciton energy, macroscopic ensembles of CdSe NPLs feature a spectrally narrow photoluminescence,[25] which can have a PLQY of 50%. Not unlike quasi-spherical CdSe NCs, as-synthesized NPLs have top and side surfaces terminated by Cd salts, which upon removal lead to the formation of localized trap states.[26] Opposite from quasi-spherical NCs, however, NPLs have a well-defined crystallography with top and side surfaces consisting of (100) facets.[27] This makes them unique model systems for testing surface chemistry−photoluminescence efficiency relations; a recent experimental and theoretical study of ligand stripping suggests that the weakest binding sites for Cd salts are found near the NPL edges.[26] Hence, a mere edge passivation should suffice to form CdSe-based NPLs with a highly efficient photoluminescence that is insensitive to ligand stripping.

In this work, we address the conjecture that Cd salts most easily desorb from edge or near-edge adsorption sites by analyzing the stripping of cadmium oleate from CdSe/CdS core/crown heteronanoplatelets. We synthesized core/crown

Received: March 19, 2020
Accepted: April 10, 2020
Published: April 10, 2020

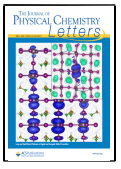

CdSe/CdS NPLs with a thickness of 4.5 monolayers (MLs) by means of a continuous injection approach, similar to what was reported in the literature.[28,29] A detailed account of the synthesis procedure is given in Supporting Information section S1. The absorption spectra of the thus obtained core and core/crown NPLs are represented in Figure 1a. Most importantly,

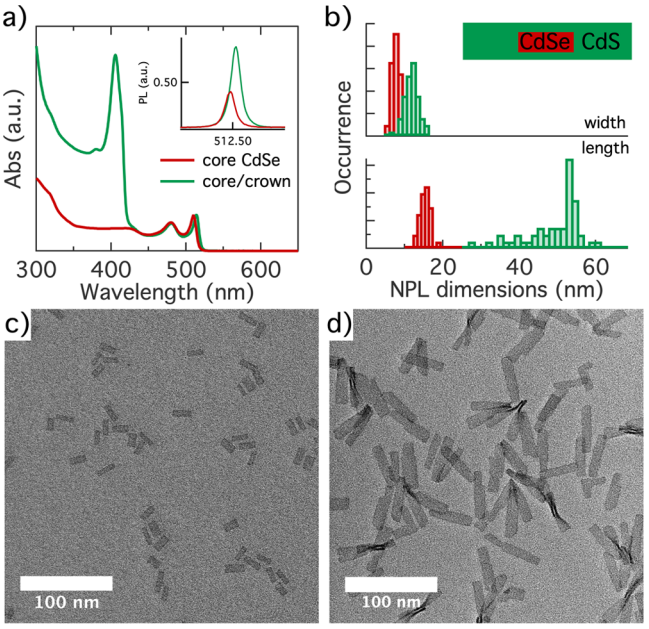

Figure 1. (a) Absorption spectrum of the initial CdSe core and final CdSe/CdS core/crown nanoplatelets (NPLs), normalized at the maximum of the heavy-hole absorption line. The inset shows the photoluminescence (PL) spectra of core and core/crown NPLs, with the area normalized to the respective PLQY. (b) Histograms of (top) the width and (bottom) the length of (red) the initial core and (green) the final core/crown NPLs. The inset shows a scheme representing the average heterostructure to scale. (c) Overview bright field TEM image of initial CdSe crown NPLs. (d) Same as panel c for the final CdSe/CdS core/crown NPLs.

the absorption spectrum of the core/crown NPLs featured both the absorption lines of the heavy- and light-hole exciton of 4.5 ML CdSe NPLs at 514 and 480 nm and the exciton line at 406 nm that is characteristic of 4.5 ML CdS NPLs.[22] On the other hand, the photoluminescence (PL) spectrum of these NPLs recorded after photoexcitation at 370 nm exhibited only a slightly red-shifted emission from CdSe excitons, not from CdS excitons (see the inset of Figure 1a and Supporting Information section S2). Finally, using the methods described in Supporting Information section S1, CdS growth increased the PLQY of the initial CdSe NPLs from 40% to 92%. Rather than a separate mixture of CdSe and CdS NPLs, these results point toward the formation of core/crown structures in which excitons formed in the CdS crown are rapidly transferred to the CdSe core, and where the CdS crown effectively passivates the remaining trap states at the CdSe NPL surface.

We evaluated the sizes as well as the morphology of the core-only and core/crown NPLs based on bright field transmission electron microscopy (TEM) images. As one can see in Figure 1b, crown growth extends the dimensions of the average NPL from 15.0 × 6.5 to 48.5 × 10.1 nm, suggesting that each CdSe edge is covered by 1.8 nm (long edges) to 9.8 nm (short edges) of CdS on average. The top view projection of multiple core/crown NPLs in Figure 1d indicates that the rectangular shape of the initial core NPLs in Figure 1c is largely conserved upon crown growth. On the basis of these dimensions, the average morphology of a core/crown NPL is depicted to scale in Figure 1b. A more detailed investigation using high-angle annular dark field (HAADF) scanning TEM (STEM) outlined in Supporting Information section S2 confirmed that 17 NPLs of a set of 19 exhibited a CdS crown on both sides of the CdSe core. However, such homogeneous crowns often featured indents or sudden thickness shifts that may leave part of the core CdSe-edge facets exposed to the surroundings. We thus conclude that the morphology of individual NPLs can show significant defects relative to the average, idealized core/crown picture shown in Figure 1b.

We applied the established solution nuclear magnetic resonance (NMR) toolbox for nanocrystal ligand analysis to further study the surface chemistry of CdSe/CdS core/crown NPLs.[30] Figure 2a depicts the ^{1}H NMR spectrum of a purified dispersion of core/crown NPLs in cyclohexane-d_{12}. Similar to the case of CdSe NPLs,[26] the spectrum features the characteristic resonances of bound oleate, which appear as well-resolved lines on top of broad pedestals. In line with existing literature, the resonances in Figure 2a were assigned to the different oleate protons as indicated in the inset of Figure 2a.[31] The CH_3 resonance **5** at 0.92 ppm and the alkene proton resonance **4** at 5.37 ppm have an integrated intensity ratio I_5/I_4 of 1.63. Because this value is close to the expected 3:2 ratio of both resonance intensities for oleic acid, we conclude that the synthesis and purification protocol implemented here result in nearly exclusively oleate-capped NPLs, despite the use of cadmium octanoate during the synthesis.

The oleate moieties found on the surface of core/crown NPLs are introduced as cadmium oleate in the final step of the synthesis. In accordance with literature studies of CdSe QDs and CdSe NPLs,[26,31] we therefore assume that the actual ligand binding to the core/crown NPL surface is best seen as cadmium oleate ($Cd(Ol)_2$). It is well-known that such so-called Z-type ligands or Lewis acids can be stripped from a metal chalcogenide surface by addition of L-type ligands or Lewis bases, such as aliphatic primary amines.[32] Taking the example of quasi-spherical CdSe NCs exposed to butylamine ($BuNH_2$), this ligand displacement can be seen as an equilibrium reaction in which amines coordinate the desorbing $Cd(Ol)_2$ complex and leave behind an empty surface site:

$$[\mathrm{CdSe}](\mathrm{Cd(Ol)_2}) + 2\mathrm{BuNH_2} \rightleftharpoons [\mathrm{CdSe}](\circ) + \mathrm{Cd(Ol)_2{-}(BuNH_2)_2} \quad (1)$$

where [CdSe] refers to the stoichiometric CdSe NCs, ($Cd(Ol)_2$) is a surface-bound cadmium oleate, and (∘) is an empty surface site. Neglecting back adsorption of $BuNH_2$, eq 1 highlights the fact that L-type driven Z-type stripping can be used to probe the $Cd(Ol)_2$ binding sites at the surface of colloidal CdSe NCs.[33]

Here, we used a $BuNH_2$ titration to quantify the binding of $Cd(Ol)_2$ to the surface of CdSe/CdS core/crown NPLs. Figure 2b illustrates the evolution of the α-CH_2 resonance **1** and the alkene resonance **4** of $Cd(Ol)_2$ during such a titration. In both cases, the appearance of narrower resonance is indicative of the formation of desorbed oleate moieties, where in particular the narrow α-CH_2 resonance **1** enables the concentration of desorbed cadmium oleate to be quantified.[26] We confirmed the co-removal of Cd during ligand stripping by elemental analysis

https://dx.doi.org/10.1021/acs.jpclett.0c00870
J. Phys. Chem. Lett. 2020, 11, 3339−3344

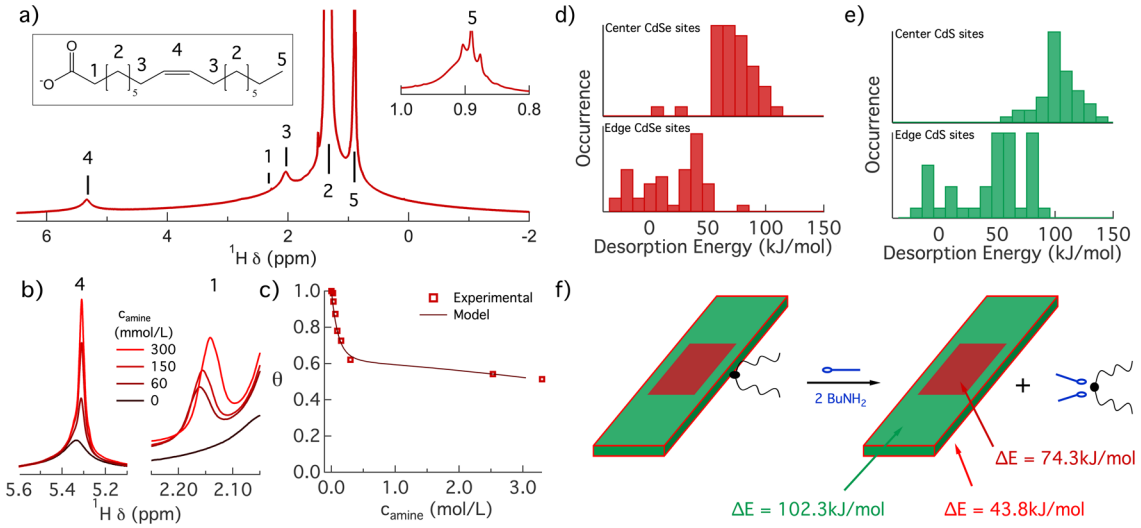

Figure 2. (a) ^{1}H NMR spectrum of a well-purified dispersion of core/crown CdSe/CdS NPLs. The proton resonances are annotated according to the numbering on the oleate moiety depicted. The inset shows a close-up of the methyl resonance **1** used in parallel with the alkene resonance to quantify the total ligand concentration. (b) Overlay of the ^{1}H NMR spectra recorded at different steps during the amine titration around (left) the alkene resonance **4** and (right) the α-CH_2 resonance **1**. In both cases, sharper resonances develop, an evolution indicative of $Cd(Ol)_2$ displacement. (c) Displacement isotherm of $Cd(Ol)_2$ depicting the bound fraction θ as a function of the concentration of $BuNH_2$ added. The markers indicate data retrieved from NMR spectra, whereas the line represents a simulated isotherm based on the two-site binding model with parameters K_1, K_2, and α as summarized in Table 1. (d) Histograms representing the computed desorption energy for the displacement of $CdCl_2$ from a model CdSe NPL by complexation with $BuNH_2$ from (top) (near)-edge sites and (bottom) facet sites. (e) Same as panel d for displacement from a model CdS NPL. (f) Schematic representation of the desorption reaction, annotated with desorption energies for the relevant binding sites of a CdSe/CdS core/crown NPL.

of the supernatant, in which case only Cd is detected after ligand stripping (see Supporting Information section S3). The displacement isotherm, showing the relative surface coverage θ of cadmium oleate at each step of the titration, is represented in Figure 2c. A detailed account of the spectra and fitting procedures underlying the isotherm determination is provided in Supporting Information section S3. We retrieve a surface coverage that quickly drops between a $BuNH_2$ concentration of 0 and 0.3 mol/L, the latter concentration corresponding to a $BuNH_2$:$Cd(Ol)_2$ equivalence of 20. At higher $BuNH_2$ concentrations, the relative surface coverage of $Cd(Ol)_2$ is largely constant, at ∼60% of the initial surface coverage. In line with previous studies of CdSe nanocrystals and CdSe NPLs, we assign these two regimes to binding site heterogeneity,[26,33] where loosely bound ligands are displaced in the initial stage of the titration, while strongly bound ligands remain on the NPL surface also at high $BuNH_2$ concentrations.

Following the idea of binding site heterogeneity, we described the adsorption isotherm by means of a two-site binding model that distinguishes weak binding sites **1** from strong binding sites **2**:

$$[CdX](Cd(Ol)_2)_1 + 2BuNH_2 \rightleftharpoons [CdX](\circ)_1 + Cd(Ol)_2{-}(BuNH_2)_2 \quad (2)$$

$$[CdX](Cd(Ol)_2)_2 + 2BuNH_2 \rightleftharpoons [CdX](\circ)_2 + Cd(Ol)_2{-}(BuNH_2)_2 \quad (3)$$

Describing the underlying nanocrystal as CdX highlights the fact that we do not distinguish at this stage of the analysis between cadmium oleate binding to undercoordinated S or Se at the core/crown surface; we will come back to this point later. Translating the set of coupled equilibrium equations into an expression for the relative surface coverage as a function of the $BuNH_2$ concentration (see Supporting Information section S3), we can simulate the measured isotherms taking the respective equilibrium constants K_1 and K_2 and the fraction α of weak binding sites as adjustable parameters. The solid line in Figure 2c represents the result of such a simulation, which was obtained by taking K_1, K_2, and α as summarized in Table 1. Similar to CdSe QDs and NPLs, Figure 2c shows that the two-site model describes the main features of the adsorption isotherm.

Table 1. Parameters of the Two-Site Binding Model for CdSe NPLs as Reported by Singh et al.[26] and CdSe/CdS Core/Crown NPLs Investigated Here

	K_1	K_2	α
CdSe NPLs	3.0	2×10^{-3}	0.375
CdSe/CdS NPLs	0.3	7×10^{-5}	0.400

To evaluate the fraction of weak binding sites **1**, we started from the consideration that CdSe/CdS core/crown NPLs have an average morphology as outlined in Figure 1b and we partitioned the total surface area into (1) edge or vertex sites and (2) facet sites. In agreement with CdSe NPLs, we defined the former as sites localized within two lattice planes of an edge. On the basis of this assumption, the idealized core/crown NPL studied here should have 34% edge sites and 66% facet sites (see Supporting Information section S3). Such an edge site fraction closely agrees with the fraction α = 0.40 of weak binding sites **1** retrieved from the two-site binding model. Possibly, the difference is related to the observed deviations from the presumed rectangular shape, which will enhance the fraction of (near)-edge sites. Even so, the agreement supports the tentative conclusion that the first stage of the isotherm

https://dx.doi.org/10.1021/acs.jpclett.0c00870
J. Phys. Chem. Lett. 2020, 11, 3339−3344

describes the displacement of $Cd(Ol)_2$ from the edges of the core/crown NPLs. In that case, the significantly lower equilibrium constant K_1 for the binding sites **1** of CdSe/CdS core/crown NPLs as compared to that of CdSe core NPLs (see Table 1) would mean that cadmium oleate binds more strongly to the CdS crown edge than to the CdSe edge of core-only NPLs.

To validate the consistency of this interpretation, we calculated the desorption energies of cadmium oleate for CdSe and CdS model NPLs using density functional theory (DFT). For computational advantage, we replaced cadmium oleate with cadmium chloride and compared the total energy of the fully relaxed NPLs before and after displacement. Panels d and e of Figure 2 represent the thus obtained desorption energy for sites near edges and on the facets of CdSe and CdS NPLs, respectively. Importantly, with an average displacement energy of 43.8 kJ/mol, the CdS-edge sites are significantly weaker than the facet sites of CdS (102.3 kJ/mol) and CdSe (74.3 kJ/mol) NPLs. Hence, we conclude that for the average core/crown NPL depicted in Figure 2f the weaker binding sites **1** effectively correspond to the CdS-edge sites.

In Figure 3a, we present PL spectra of two dispersions of core/crown NPLs during a titration with $BuNH_2$, where intensities were normalized relative to the initial, purified dispersion. We used an excitation wavelength of 460 nm to ensure that excitons are exclusively formed within the CdSe core. For an unoptimized core/crown NPL sample, in which most NPLs have an incomplete crown (see Supporting Information section S2), the addition of small amounts of $BuNH_2$ leads to a rapid loss of the PL, a result that closely agrees with the loss of PL upon addition of $BuNH_2$ to core CdSe NPLs.[26] On the other hand, upon addition of $BuNH_2$ to CdSe/CdS core/crown dispersions synthesized with the optimized procedure, the initial rapid decrease in the PL efficiency gives way to a plateau where the PLQY levels off at a sample-dependent level of 30% or even 45% of the initial value (see Figure 3b). Upon ligand stripping, the PL spectrum remains characteristic of CdSe exciton recombination, even if slight spectral changes suggest a preferential quenching of the blue side of the emission line (see Supporting Information section S4).

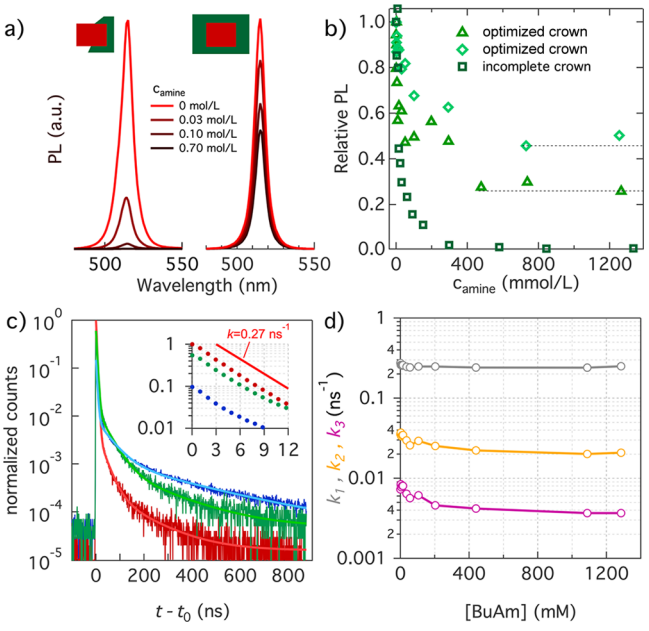

Figure 3. (a) PL spectra of CdSe/CdS core/crown NPLs at different steps during a $BuNH_2$ titration, including (left) incomplete core/crown and (right) optimized core/crown NPLs. For both samples, PL spectra have been normalized relative to the initial spectrum, i.e., before $BuNH_2$ addition. (b) Evolution of the relative PLQY during $BuNH_2$ titration for (squares) NPLs with an incomplete crown and (diamonds and triangles) two different samples synthesized following the optimized procedure. (c) Transient PL of the (red) initial sample, (green) the sample after addition of 55 mM $BuNH_2$, and (blue) the sample after addition of 1285 mM $BuNH_2$. Lighter color lines correspond to the three-exponential fits. The inset is a close-up of the first 15 ns of the decay with the traces normalized to their respective PLQY. The reference line represents a single-exponential decay with an emission rate of 0.27 ns^{-1}. (d) Different rate constants obtained by fitting a three-exponential decay to the transient PL as a function of $BuNH_2$ concentration.

The loss of PLQY upon $BuNH_2$ addition can reflect either a gradual reduction of the emission efficiency for each NPL or the progressive formation of a dark fraction within the ensemble, each a possibility that can be distinguished by time-resolved PL. Figure 3c therefore represents PL transients recorded on a CdSe/CdS core/crown sample at different stages of a $BuNH_2$ titration after photoexcitation with 460 nm pulses. As one can see, the PL transient $I(t)$ of the initial sample, which had a PLQY of 90%, is dominated by a single-exponential decay component that gives way to a minor tail of delayed emission. Importantly, the decay rate k_1 of the dominant component amounts to 0.27 ns^{-1}, a typical number for radiative exciton recombination in NPLs.[34] Starting from this assignment, we attribute the delayed emission to carrier capture-and-release processes that slow exciton recombination without inducing additional emission bands in the PL spectrum. Interestingly, the transients recorded after addition of 55 mM (green) and 1285 mM (blue) $BuNH_2$, concentrations that correspond to the region of the initial PL drop and the PL plateau, feature the same initial single-exponential decay followed by a tail of delayed emission that exhibits, by and large, the same decay profile.

Given their similar time dependence, we analyzed all PL transients by a fit to a three-exponential decay (see Supporting Information section S4). Figure 3d represents the thus obtained rate constants. In line with the qualitative observation, the rate of the fastest component (k_1), which we assigned to direct radiative exciton recombination, is independent of the $BuNH_2$ concentration while the rate of the slower components drops by a factor of ≤ 2. Importantly, none of these rate constants increases, which suggests that for the NPLs that keep emitting throughout the titration, competition with nonradiative decay components remains absent. More quantitatively, the combination of amplitudes and rates obtained through the fit indicates that for the initial sample, 95% of the emitted photons are contained in the direct radiative exciton component. For samples in the PL plateau, this fraction is still 64% (see Supporting Information section S4). Hence, direct radiative exciton recombination remains the dominant emission component for the emitting NPLs during a $BuNH_2$ titration. Accordingly, we conclude that $BuNH_2$ titration splits the NPL population into two fractions. For the first fraction, ligand stripping leads to the complete quenching of the PL, a process that accounts for the observed PL efficiency drop. For the second, $BuNH_2$ addition leads to only minor changes in the PL dynamics without affecting the radiative recombination rate.

https://dx.doi.org/10.1021/acs.jpclett.0c00870
J. Phys. Chem. Lett. 2020, 11, 3339−3344

Bringing together the results of the structural characterization, the evolution of the surface chemistry, the steady-state and time-resolved PL during $BuNH_2$ titration, and the theoretical analysis of the $Cd(Ol)_2$ binding energy leads to a consistent picture of the relation between surface chemistry and optoelectronic properties of CdSe core and CdSe/CdS core/crown NPLs. For both systems, the combination of $Cd(Ol)_2$ displacement and the theoretical estimates of the $Cd(Ol)_2$ binding energy indicates that ligands are preferentially stripped from (near)-edge binding sites. Importantly, CdSe/CdS core/crown NPLs have a straddling band alignment that keeps the exciton localized within the CdSe core.[25] Under such conditions, ligand stripping from the CdS edge of core/crown NPLs should not affect the radiative exciton recombination provided a fully homogeneous crown is grown around the CdSe core. The comparison of PL quenching in defective, and optimized core/crown NPLs confirms this point. Defective core/crown NPLs behave like CdSe core NPLs, indicating that indeed part of the CdSe edge remains unpassivated. On the other hand, optimized core/crown NPLs preserve a significant fraction of the original PL efficiency, a result we assign to the combined presence of NPLs with a defective and a homogeneous CdS crown as confirmed by STEM-HAADF imaging. The identification of well and poorly crowned NPLs in an ensemble is further confirmed by transient PL during ligand stripping, which also gave evidence of two populations. At this point, assigning the emitting fraction to perfectly crowned NPLs and the dark fraction to imperfectly crowned NPLs becomes straightforward. Interestingly, the preferential loss of the blue side of the exciton emission supports this conclusion as incompletely crowned NPLs will have experienced, on average, a smaller red shift.

In summary, this work addresses the interrelation between surface chemistry and optoelectronic properties in colloidal semiconductor nanocrystals using core/crown CdSe/CdS NPLs capped by $Cd(Ol)_2$ as a model system. Unlike CdSe core NPLs, such core/crown NPLs can retain up to 45% of their original PL upon progressive $Cd(Ol)_2$ stripping. This different behavior confirms that (100) facets passivated by Z-type ligands such as $Cd(Ol)_2$ lead to nanocrystals with clean HOMO−LUMO gaps, i.e., without localized midgap states. Moreover, Z-type ligand binding to such a facet is strong and withstands the relatively harsh ligand stripping environment created by $BuNH_2$ addition. This conclusion explains why CdSe core and CdSe/CdS core/crown NPLs can be grown with a PLQY of 50 to nearly 100% without full passivation by an inorganic shell. Opposite from the binding sites on the (100) facet, we find that (near)-edge binding sites are weaker and more vulnerable to ligand displacement. In the case of two-dimensional NPLs, such sites are well-localized on the NPL surface and edge passivation by the mere growth of a CdS crown suffices to turn CdSe NPLs into more robust CdSe/CdS core/crown structures. For spherical NCs, on the other hand, edge sites are plentiful and distributed over the entire NC surface. As a result, homogeneous shelling is typically the most staightforward surface passivation approach. Even if the saturation of the surface with Z-type ligands can suffice to attain a nearly 100% PLQY, our work suggests that such NCs remain prone to PL quenching because the ubiquitous edge sites will bind Z-type ligands more weakly.

■ ASSOCIATED CONTENT

Supporting Information

The Supporting Information is available free of charge at https://pubs.acs.org/doi/10.1021/acs.jpclett.0c00870.

(1) A detailed description of experimental conditions, (2) a study of CdSe crown growth, (3) data and models for $BuNH_2$-induced $Cd(Ol)_2$ stripping, and (4) an overview of the steady-state and transient photoluminescence spectroscopy (PDF)

■ AUTHOR INFORMATION

Corresponding Author

Zeger Hens − *Physics and Chemistry of Nanostructures and Center for Nano and Biophotonics, Ghent University, 9000 Ghent, Belgium;* orcid.org/0000-0002-7041-3375; Email: zeger.hens@ugent.be

Authors

Jari Leemans − *Physics and Chemistry of Nanostructures and Center for Nano and Biophotonics, Ghent University, 9000 Ghent, Belgium*

Shalini Singh − *Physics and Chemistry of Nanostructures and Center for Nano and Biophotonics, Ghent University, 9000 Ghent, Belgium;* orcid.org/0000-0001-8607-8383

Chen Li − *Electron Microscopy for Materials Research (EMAT), University of Antwerp, 2020 Antwerp, Belgium*

Stephanie Ten Brinck − *Department of Theoretical Chemistry, Faculty of Science, Vrije Universiteit Amsterdam, 1081 HV Amsterdam, The Netherlands*

Sara Bals − *Electron Microscopy for Materials Research (EMAT), University of Antwerp, 2020 Antwerp, Belgium;* orcid.org/0000-0002-4249-8017

Ivan Infante − *Department of Nanochemistry, Istituto Italiano di Tecnologia, 16163 Genova, Italy; Department of Theoretical Chemistry and Amsterdam Center for Multiscale Modeling (ACMM), VU University Amsterdam, 1081 HV Amsterdam, The Netherlands;* orcid.org/0000-0003-3467-9376

Iwan Moreels − *Physics and Chemistry of Nanostructures and Center for Nano and Biophotonics, Ghent University, 9000 Ghent, Belgium;* orcid.org/0000-0003-3998-7618

Complete contact information is available at: https://pubs.acs.org/10.1021/acs.jpclett.0c00870

Notes

The authors declare no competing financial interest.

■ ACKNOWLEDGMENTS

Z.H. and S.B. acknowledge support by SIM-Flanders (SBO-QDOCCO). Z.H. acknowledges support by FWO-Vlaanderen (research project 17006602). Z.H. and I.M. acknowledge support by Ghent University (GOA n° 01G01019). J.L. acknowledges FWO-vlaanderen for a fellowship (SB Ph.D. fellow at FWO). S.S. acknowledges FWO postdoctoral funding (FWO17/PDO/184). This project has further received funding from the European Research Counsil under the European Union's Horizon 2020 research and innovation programme (ERC Consolidator Grant 815128 REALNANO and Starting Grant 714876 PHOCONA). The computational work was carried out on the Dutch national e-infrastructure with the support of the SURF Cooperative.

REFERENCES

(1) Talapin, D. V.; Lee, J.-S.; Kovalenko, M. V.; Shevchenko, E. V. Prospects of Colloidal Nanocrystals for Electronic and Optoelectronic Applications. *Chem. Rev.* **2010**, *110*, 389−458.

(2) Kovalenko, M. V.; Manna, L.; Cabot, A.; Hens, Z.; Talapin, D. V.; Kagan, C. R.; Klimov, V. I.; Rogach, A. L.; Reiss, P.; Milliron, D. J.; et al. Prospects of Nanoscience with Nanocrystals. *ACS Nano* **2015**, *9*, 1012−1057.

(3) Moon, H.; Lee, C.; Lee, W.; Kim, J.; Chae, H. Stability of Quantum Dots, Quantum Dot Films, and Quantum Dot Light-Emitting Diodes for Display Applications. *Adv. Mater.* **2019**, *31*, 1804294.

(4) Hines, D. A.; Kamat, P. V. Recent Advances in Quantum Dot Surface Chemistry. *ACS Appl. Mater. Interfaces* **2014**, *6*, 3041−3057.

(5) Yu, M.; Fernando, G.; Li, R.; Papadimitrakopoulos, F.; Shi, N.; Ramprasad, R. First Principles Study of CdSe Quantum Dots: Stability, Surface Unsaturations, and Experimental Validation. *Appl. Phys. Lett.* **2006**, *88*, 231910.

(6) Dabbousi, B. O.; Rodriguez-Viejo, J.; Mikulec, F. V.; Heine, J. R.; Mattoussi, H.; Ober, R.; Jensen, K. F.; Bawendi, M. G. (CdSe)ZnS Core-Shell Quantum Dots: Synthesis and Characterization of a Size Series of Highly Luminescent Nanocrystallites. *J. Phys. Chem. B* **1997**, *101*, 9463−9475.

(7) Talapin, D. V.; Rogach, A. L.; Kornowski, A.; Haase, M.; Weller, H. Highly Luminescent Monodisperse CdSe and CdSe/ZnS Nanocrystals Synthesized in a Hexadecylamine-Trioctylphosphine Oxide-Trioctylphosphine Mixture. *Nano Lett.* **2001**, *1*, 207−211.

(8) Haubold, S.; Haase, M.; Kornowski, A.; Weller, H. Strongly Luminescent InP/ZnS Core−Shell Nanoparticles. *ChemPhysChem* **2001**, *2*, 331−334.

(9) Peng, X.; Schlamp, M. C.; Kadavanich, A. V.; Alivisatos, A. P. Epitaxial Growth of Highly Luminescent CdSe/CdS Core/Shell Nanocrystals with Photostability and Electronic Accessibility. *J. Am. Chem. Soc.* **1997**, *119*, 7019−7029.

(10) Knowles, K. E.; Frederick, M. T.; Tice, D. B.; Morris-Cohen, A. J.; Weiss, E. A. Colloidal Quantum Dots: Think Outside the (Particle-in-a-)Box. *J. Phys. Chem. Lett.* **2012**, *3*, 18−26.

(11) Kirkwood, N.; Monchen, J. O.; Crisp, R. W.; Grimaldi, G.; Bergstein, H. A.; du Fossé, I.; van der Stam, W.; Infante, I.; Houtepen, A. J. Finding and Fixing Traps in II−VI and III−V Colloidal Quantum Dots: The Importance of Z-Type Ligand Passivation. *J. Am. Chem. Soc.* **2018**, *140*, 15712−15723.

(12) Pan, J.; Shang, Y.; Yin, J.; De Bastiani, M.; Peng, W.; Dursun, I.; Sinatra, L.; El-Zohry, A. M.; Hedhili, M. N.; Emwas, A.-H.; et al. Bidentate Ligand-Passivated CsPbI3 Perovskite Nanocrystals for Stable Near-Unity Photoluminescence Quantum Yield and Efficient Red Light-Emitting Diodes. *J. Am. Chem. Soc.* **2018**, *140*, 562−565.

(13) Munro, A. M.; Jen-La Plante, I.; Ng, M. S.; Ginger, D. S. Quantitative Study of the Effects of Surface Ligand Concentration on CdSe Nanocrystal Photoluminescence. *J. Phys. Chem. C* **2007**, *111*, 6220−6227.

(14) Bullen, C.; Mulvaney, P. The Effects of Chemisorption on the Luminescence of CdSe Quantum Dots. *Langmuir* **2006**, *22*, 3007−3013.

(15) Houtepen, A. J.; Hens, Z.; Owen, J. S.; Infante, I. On the Origin of Surface Traps in Colloidal II−VI Semiconductor Nanocrystals. *Chem. Mater.* **2017**, *29*, 752−761.

(16) Giansante, C.; Infante, I. Surface Traps in Colloidal Quantum Dots: A Combined Experimental and Theoretical Perspective. *J. Phys. Chem. Lett.* **2017**, *8*, 5209−5215.

(17) Stein, J. L.; Mader, E. A.; Cossairt, B. M. Luminescent InP Quantum Dots with Tunable Emission by Post-Synthetic Modification with Lewis Acids. *J. Phys. Chem. Lett.* **2016**, *7*, 1315−1320.

(18) Joo, J.; Son, J. S.; Kwon, S. G.; Yu, J. H.; Hyeon, T. Low-Temperature Solution-Phase Synthesis of Quantum Well Structured CdSe Nanoribbons. *J. Am. Chem. Soc.* **2006**, *128*, 5632−5633.

(19) Son, J. S.; Park, K.; Kwon, S. G.; Yang, J.; Choi, M. K.; Kim, J.; Yu, J. H.; Joo, J.; Hyeon, T. Dimension-Controlled Synthesis of CdS Nanocrystals: From 0D Quantum Dots to 2D Nanoplates. *Small* **2012**, *8*, 2394−2402.

(20) Son, J. S.; Yu, J. H.; Kwon, S. G.; Lee, J.; Joo, J.; Hyeon, T. Colloidal Synthesis of Ultrathin Two-Dimensional Semiconductor Nanocrystals. *Adv. Mater.* **2011**, *23*, 3214−3219.

(21) Ithurria, S.; Dubertret, B. Quasi 2D Colloidal CdSe Platelets with Thicknesses Controlled at the Atomic Level. *J. Am. Chem. Soc.* **2008**, *130*, 16504−16505.

(22) Ithurria, S.; Tessier, M.; Mahler, B.; Lobo, R.; Dubertret, B.; Efros, A. L. Colloidal Nanoplatelets with Two-Dimensional Electronic Structure. *Nat. Mater.* **2011**, *10*, 936.

(23) Gerdes, F.; Navío, C.; Juárez, B. H.; Klinke, C. Size, Shape, and Phase Control in Ultrathin CdSe Nanosheets. *Nano Lett.* **2017**, *17*, 4165−4171.

(24) Christodoulou, S.; Climente, J. I.; Planelles, J.; Brescia, R.; Prato, M.; Martín-García, B.; Khan, A. H.; Moreels, I. Chloride-Induced Thickness Control in CdSe Nanoplatelets. *Nano Lett.* **2018**, *18*, 6248−6254.

(25) Tessier, M. D.; Javaux, C.; Maksimovic, I.; Loriette, V.; Dubertret, B. Spectroscopy of Single CdSe Nanoplatelets. *ACS Nano* **2012**, *6*, 6751−6758.

(26) Singh, S.; Tomar, R.; Ten Brinck, S.; De Roo, J.; Geiregat, P.; Martins, J. C.; Infante, I.; Hens, Z. Colloidal CdSe Nanoplatelets, A Model for Surface Chemistry/Optoelectronic Property Relations in Semiconductor Nanocrystals. *J. Am. Chem. Soc.* **2018**, *140*, 13292−13300.

(27) Lhuillier, E.; Pedetti, S.; Ithurria, S.; Nadal, B.; Heuclin, H.; Dubertret, B. Two-Dimensional Colloidal Metal Chalcogenides Semiconductors: Synthesis, Spectroscopy, and Applications. *Acc. Chem. Res.* **2015**, *48*, 22−30.

(28) Tessier, M. D.; Spinicelli, P.; Dupont, D.; Patriarche, G.; Ithurria, S.; Dubertret, B. Efficient Exciton Concentrators Built from Colloidal Core/Crown CdSe/CdS Semiconductor Nanoplatelets. *Nano Lett.* **2014**, *14*, 207−213.

(29) Prudnikau, A.; Chuvilin, A.; Artemyev, M. CdSe−CdS Nanoheteroplatelets with Efficient Photoexcitation of Central CdSe Region through Epitaxially Grown CdS Wings. *J. Am. Chem. Soc.* **2013**, *135*, 14476−14479.

(30) Hens, Z.; Martins, J. C. A Solution NMR Toolbox for Characterizing the Surface Chemistry of Colloidal Nanocrystals. *Chem. Mater.* **2013**, *25*, 1211−1221.

(31) Fritzinger, B.; Capek, R. K.; Lambert, K.; Martins, J. C.; Hens, Z. Utilizing Self-Exchange To Address the Binding of Carboxylic Acid Ligands to CdSe Quantum Dots. *J. Am. Chem. Soc.* **2010**, *132*, 10195−10201.

(32) Anderson, N. C.; Hendricks, M. P.; Choi, J. J.; Owen, J. S. Ligand Exchange and the Stoichiometry of Metal Chalcogenide Nanocrystals: Spectroscopic Observation of Facile Metal-Carboxylate Displacement and Binding. *J. Am. Chem. Soc.* **2013**, *135*, 18536−18548.

(33) Drijvers, E.; De Roo, J.; Martins, J. C.; Infante, I.; Hens, Z. Ligand Displacement Exposes Binding Site Heterogeneity on CdSe Nanocrystal Surfaces. *Chem. Mater.* **2018**, *30*, 1178−1186.

(34) Kunneman, L. T.; Schins, J. M.; Pedetti, S.; Heuclin, H.; Grozema, F. C.; Houtepen, A. J.; Dubertret, B.; Siebbeles, L. D. Nature and Decay Pathways of Photoexcited States in CdSe and CdSe/CdS Nanoplatelets. *Nano Lett.* **2014**, *14*, 7039−7045.

https://dx.doi.org/10.1021/acs.jpclett.0c00870
J. Phys. Chem. Lett. 2020, 11, 3339−3344